Pushing and pulling on OH^- and H_3O^+ with electric fields across water's surface

Kamal K. Ray[1], Aditya Limaye[2], Ankur Saha[1], Ka Chon Ng[1], Adam P. Willard*[2], and Heather C. Allen*[1]

[1] The Ohio State University, Department of Chemistry and Biochemistry, Columbus, OH 43210.
[2] MIT, Department of Chemistry, Cambridge, MA 02139.
*allen@chemistry.ohio-state.edu
*awillard@mit.edu

We use second harmonic generation spectroscopy, molecular dynamics simulation, and theoretical modeling to study the response of the neat liquid water-air interface to changes in the potential of an external electrode positioned above the liquid. We observe a parabolic dependence of second harmonic intensity on applied potential, indicating that water's net interfacial dipole responds linearly. We also observe a minimum intensity when the potential is tuned to a specific positive value. Interpreting this minimum based on the macroscopic electrostatic potential profile yields misleading physical conclusions because it neglects the internal bias exerted on molecular orientations by the excess surface concentrations of OH^- or H_3O^+. We thus find that water's net interfacial dipole orientation is primarily responsive to the effects of these ionic species rather than the external electric field.

The physical, chemical, and biological properties of the liquid water-air interface are connected to, yet distinct from, those of the bulk liquid. These connections and distinctions must be characterized before we can fully understand the wide range of fundamental processes that are known to occur preferentially, or even exclusively, at the liquid water-air interface. In its most prevalent role - that of a solvent - water's properties are determined by the nanoscale structure and dynamics of the molecular hydrogen bonding network [1-3]. At an interface, this network is constrained and distorted, leading to anisotropy in the orientational distributions of water molecules as well as the electrostatic and dielectric properties that these distributions determine [4-7]. Resolving the details of these interfacial properties is important because they have a significant influence on interfacial solvation and transport (especially for charged species) as well as the thermodynamics and kinetics of aqueous interfacial chemical reactions, such as those that regulate the composition of our oceans and atmosphere, or the processes that control the assembly of supramolecular structures [8-14].

Over the last several decades, numerous scientific studies have been aimed at characterizing the molecular structure and associated electrostatic properties of the liquid water interface [15-17]. Despite these efforts, much remains to be understood about how the solvent properties of liquid water surfaces differ from those of the bulk and what those differences reveal about the interfacial molecular structure [18-22]. Water surface properties are difficult to measure because common experimental probes cannot isolate the signal of the interface from that of the bulk, and those that can are noisy and/or report indirectly on the microscopic details of the surface. Furthermore, the interpretation of interface-sensitive experiments is complicated by uncertainty in experimental probe-depth and limited reliability of theoretical models for treating interfacial systems [23,24]. Most notably, the various empirical force fields that are routinely used in molecular dynamics (MD) simulation, which are parameterized based on bulk properties, differ in their predictions of many key features of water's interfacial molecular structure [21,25-29].

The molecular structure of the liquid water interface can be studied by measuring its polarization response under an applied electric field [30-35]. Such a field interacts with the dipole moment of water molecules and biases their orientational alignment. Second harmonic generation (SHG) spectroscopy is sensitive to the net interfacial dipole [36-39] and can thus report upon the average molecular alignment of the water surface and how it changes under various external fields [30-34]. By analyzing these changes and evaluating them in the context of

simple theoretical models, it is possible to gain information about the configurational statistics of interfacial water molecules and thereby infer details of interfacial molecular structure that are not apparent via unbiased measurement alone.

Results and discussion

Here we utilize SHG spectroscopy to probe the response of the neat water-air interface to a tunable externally applied electric field, building upon the work of Schmid, Hurd, and Snavely [30,34]. The electric field is controlled by varying the potential of an electrode positioned in the air above a sample of neat liquid water; a second grounded electrode is directly below in the liquid (Fig. 1). We regard that changes in the overall SHG intensity under applied external potential are due to changes in the net interfacial dipole.[38] We interpret the results of these experiments by modeling the interface as a linearly responding dipole field. We assign the details of this model based on analysis of classical molecular dynamics simulation (as described in more detail in the SI). We assert that the dipole field is subject to a combination of an external field, originating from the electrodes, and an internal field, originating from an excess concentration of OH^- or H_3O^+ that are driven to the surface by the external field. Even at moderate applied potentials (e.g., ~10-100 V) the excess surface concentrations of these ionic species are predicted to be many orders magnitude larger than that predicted based on their equilibrium bulk concentrations. We then assume this excess surface charge contributes capacitive fields across the region of the interface.

Because we are only concerned with electric fields perpendicular to the interface, we refer to the field as a single scalar gleaned from dotting the electric field vector onto an interface normal pointing from the air side into the liquid water. Hence, a positive (negative) field corresponds to the air electrode being held at a positive (negative) potential relative to the grounded water electrode. The experimental results, plotted in Fig. 1B, reveal the response in SHG intensity, using a *pp* polarization combination, to positive and negative external potential. The SHG intensity is approximately parabolic, with a minimum at a positive potential of approximately 2.8 kV. Second harmonic photons are generated from environments that lack centrosymmetry, such as the liquid-water interface.[37] Since SHG signal intensity is predicted to exhibit a quadratic dependence on the net interfacial dipole, the parabolic dependence in Fig. 1B implies that the net interfacial dipole varies linearly with the applied electric field. This linear response behavior suggests that the electric fields incident upon the water-air interface are not strong enough to significantly restructure the interfacial hydrogen bonding network of water; rather, they simply induce subtle changes in the orientational preference of interfacial water molecules not detectable by the complementary nonlinear optical probe of vibrational sum-frequency generation spectroscopy (SI).

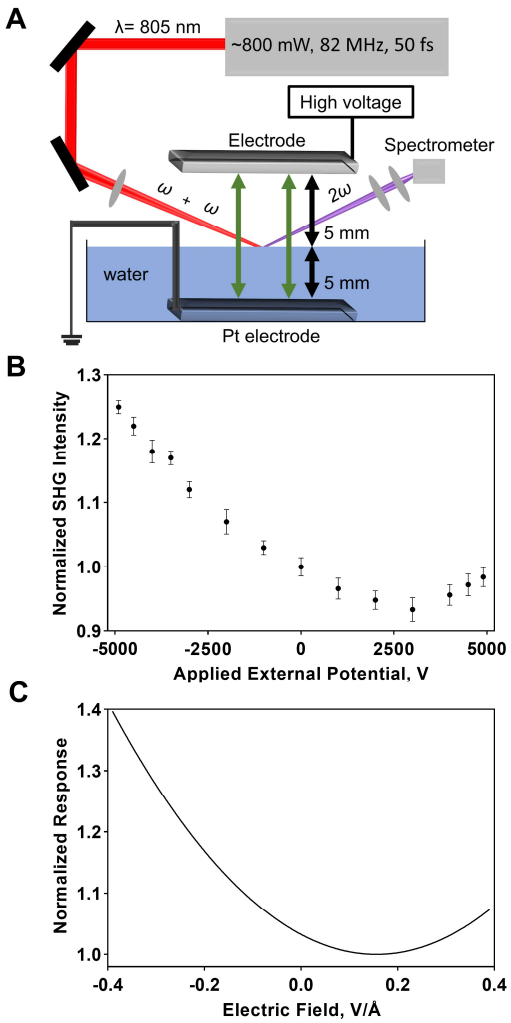

Fig. 1. Water – air interfacial response to an applied external potential. (A) Schematic diagram of the high voltage second harmonic generation set-up. The pulsed laser (Ti:sapphire, λ= 805 ± 10 nm,

repetition rate ~82 MHz, <50 fs, vertically polarized) generates the second order intensity that is detected (p-polarized) by the EM-CCD. The high voltage set up is comprised of an air-phase electrode (DC-powered steel plate; 25 mm x 20 mm) and a counter electrode in the condensed-phase (grounded parallel platinum plate; 25 mm x 22 mm). (B) Experimental normalized second harmonic generation intensity (sample signal divided by the reference signal at unbiased condition) with the externally applied electric potential of -5 kV to +5 kV revealing an intensity minimum at applied bias of ~+2.8 kV. (C) Theoretical model of the normalized squared interfacial dipole and parameters extracted from classical MD simulation.

Experimentally, we control the potential difference between the two electrodes, yet the SHG intensity is dependent on the resulting electric field incident across the water interface. Translating the applied potential to a field requires a theoretical model based on specific physical assumptions. Such a model describes how the average electrostatic potential varies in space along the direction separating the two electrodes, which sets the boundary conditions, as illustrated in Fig. 2. The average electric field at any point within the system is thus given by the potential gradient at that point.

We begin by considering a Gouy-Chapman model of interfacial fields[40,41], in which the mobile OH^- and H_3O^+ ions in water screen the potential drop over microscopic lengths at the water-air and water-electrode interfaces, also illustrated in Fig. 2. Accounting for the screening effects of OH^- and H_3O^+, we model the water region as an electrolyte solution with a screening length of 960 nm, as appropriate for the experimental pH and temperature. Applying Gouy-Chapman theory yields an estimated interfacial field strength of ± 0.13 V/ Å for the experimental maximum in the applied potentials of ± 5 kV. Based on insight from molecular simulations, this magnitude of field would not be expected to cause any significant restructuring of the hydrogen bond network (SI). This expectation is further corroborated by our vibrational sum-frequency generation spectra, under polarized conditions, that show no significant difference in the orientation of the OH dangling bond nor changes in the OH stretching region under applied potentials (SI).

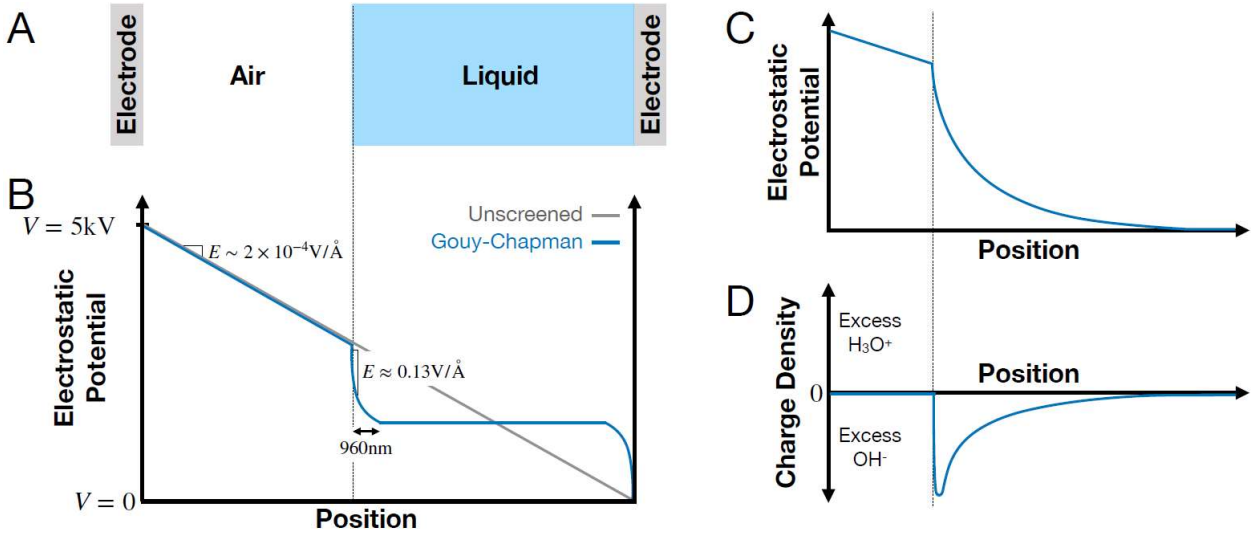

***Fig. 2**. Illustrating the Gouy-Chapman model as applied to the experimental setup. (A) A schematic of the experimental setup with a variable potential electrode on the left-hand side and a grounded (V=0) electrode on the right-hand side. (B) The formation of a screening layer at both liquid boundaries leads to an attenuation of the potential at the water interfaces, highlighted here at the maximum positive potential. As indicated, the fields predicted in these screening regions are significantly larger than that originating from the unscreened electrodes (grey line). (C-D) An illustration of the potential profile and corresponding*

charge density profile at the water-air interface for positive applied potential. OH^- ions are drawn to the interface by the positive air electrode lead to a diffuse region of excess negative charge.

If the parabolic profile of the SHG intensity corresponds to linear variation in the net interfacial dipole, then the position of the minimum reveals the state for which the interface carries no net dipole. According to the Gouy-Chapman model, as described above, this neutralizing field is positive, corresponding a positively charged air electrode. The Gouy-Chapman model thus predicts, as illustrated in the left-hand side of Fig. 3, that the net dipole under zero applied potential corresponds to molecular configurations with hydrogens pointed up, away from the bulk liquid. Notably, this prediction is in disagreement with the prevailing understanding that the average orientation of water molecules at the water-air interface is with hydrogens pointed slightly down. This understanding has been developed over several decades from various experimental and theoretical studies.[39,42-50]

If one assumes, as is well accepted over the last decade, that the interfacial dipole in the unbiased state (at zero applied potential) corresponds to an average hydrogen down molecular orientation (albeit minimally), then the interfacial field required to neutralize the net dipole would be expected to favor a net hydrogen up configuration. Such a field would apparently require a negatively charged external electrode. Given that this outcome is not consistent with the well documented hydrogen down orientation, we propose the unorthodox interpretation that water's interfacial hydrogen bonding network is primarily responsive to the internal molecular fields that originate from excess concentrations of OH^- or H_3O^+ and not from the average macroscopic fields that are predicted based on analysis of the average charge density. The bare (unscreened) external fields originating from the electrodes are miniscule, on the order of 5×10^{-5} V/Å, and thus cannot independently account for an observable change to water's net interfacial dipole. However, when these small fields are applied over an entire liquid slab, excess OH^- and H_3O^+ are driven to opposing boundaries in concentrations that massively exceed that of the bulk. We propose here that the influence of the induced excess surface hydroxide or hydronium concentrations, in each case, play a primary role in directing the dipoles of water molecules in the region of the interface.

At +2.8 kV the positively charged electrode will drive the formation of an excess layer of OH^- at the liquid water-air interface and, as we propose, the fields from this excess will direct water molecules to effectively neutralize the net interfacial dipole. We can estimate the excess negative surface charge required to achieve this neutralization by modeling the average interfacial dipole as a linear responding field that obeys the following relationship,

$$\langle \bar{\mu} \rangle \propto \langle \bar{\mu} \rangle_0 + \alpha E,$$

where $\bar{\mu}$ represents the net dipole in units of the dipole moment of a molecule in the liquid, E is the strength of the electric field perpendicular to the interface, and $\alpha = 0.6\,\text{Å}V^{-1}$ is the dipole susceptibility based on molecular dynamics simulations that are described in the SI. We assume a value for the unbiased dipole of $\langle \bar{\mu} \rangle_0 = 0.055$, corresponding to a slight hydrogen down configuration (SI). We thus estimate that an internal electric field of $-0.13V/\text{Å}$ created by hydroxide repartitioning is sufficient to produce a net zero interfacial dipole field.

Assuming that ions form a capacitive charge layer by occupying the outer surface of the liquid, such a field requires an excess OH^- concentration at the surface of approximately $3 \times 10^{-9}\,\text{mol/cm}^2$, which is significantly larger than that from the assumed bulk value of neat water autoionization.

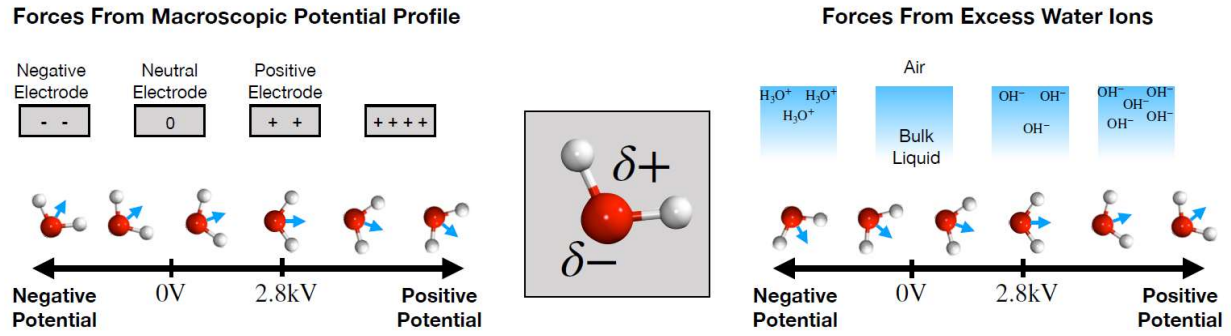

Figure 3. Left panel. Outcome from the traditional electrostatics approach. At zero bias, dipole orientation (of hydrogen-up) is inconsistent with well-vetted literature. Right panel. Outcome from including the microscopic character of the interface that is comprised of OH^- and H_3O^+ from the autoionization of neat water. At zero bias, derived from an understanding of the experimental minimum at +2.8 kV, the net dipole orientation of hydrogen-down configurations is expected.

In the absence of external stabilization by an applied external field, such a surface excess implies that OH^- is approximately 20 k_BT more stable than H_3O^+ at the surface. Based on a simple model for the electrostatic potential profile in the experimental apparatus, this magnitude of stabilization can in fact be accessed at rather modest applied potentials of ~10 V. The apparent need for larger potentials (~10^3 V) to achieve this stabilization indicates that the interfacial solvation of OH^- and H_3O^+ is more complicated than assumed in traditional screening models. We thus assert that ion correlations and changes to the hydrogen bonding network at large OH^- or H_3O^+ concentrations impose free energetic costs that can only be overcome at the larger potentials we have applied here.

The specific responsiveness of water's interfacial dipole to internal fields from interfacial concentrations of OH^- and H_3O^+ has an important physical implication. If our interpretation is correct, then interfacial internal fields that are relevant to molecular structure are not necessarily those predicted by traditional mean-field theories (e.g., Gouy-Chapman theory). In other words, the fields implied by the average potential profile cannot be applied to predict interfacial dipole properties. Further theoretical developments that identify the origins of these molecular effects and incorporate them into existing theoretical models are thus needed to advance our ability to interpret experimental data.

Conclusion

In this work we present a combined experimental and theoretical study to understand the inherent structure and net dipole orientation of water molecules at the water - air interface at room temperature and at atmospheric pressure. Our theoretical modeling analyses of the second harmonic generated parabolic intensity, and offset minimum at positive potential, resulting from the application of an electric potential perpendicular to the surface with traditional electrostatics fails to adequately describe our experimental results. Our interpretation of the observed experimental signal minimum, shown at a positive bias, suggests that the fields implied by a traditional device-scale potential profile are inconsistent with the current paradigm of hydrogen-down structure of the water interface. We thus conclude through an approach that incorporates the electrolyte properties of neat water that water's interfacial molecular structure is primarily responsive to internal fields originating from excess OH^- or H_3O^+ at the surface.

.

References:

1 Ohmine, I. & Saito, S. Water Dynamics: Fluctuation, Relaxation, and Chemical Reactions in Hydrogen Bond Network Rearrangement. *Accounts of Chemical Research* **32**, 741-749, doi:10.1021/ar970161g (1999).

2 Ohmine, I. & Tanaka, H. Fluctuation, relaxations, and hydration in liquid water. Hydrogen-bond rearrangement dynamics. *Chem. Rev.* **93**, 2545-2566, doi:10.1021/cr00023a011 (1993).

3 Smith, J. D. *et al.* Energetics of Hydrogen Bond Network Rearrangements in Liquid Water. *Science* **306**, 851-853, doi:10.1126/science.1102560 (2004).

4 Jungwirth, P., Finlayson-Pitts, B. J. & Tobias, D. J. Introduction: Structure and Chemistry at Aqueous Interfaces. *Chem. Rev.* **106**, 1137-1139, doi:10.1021/cr040382h (2006).

5 Goh, M. C. *et al.* Absolute orientation of water molecules at the neat water surface. *J. Phys. Chem.* **92**, 5074-5075, doi:10.1021/j100329a003 (1988).

6 Shen, Y. R. & Ostroverkhov, V. Sum-frequency vibrational spectroscopy on water interfaces: polar orientation of water molecules at interfaces. *Chem Rev* **106**, 1140-1154 (2006).

7 Nicodemus, R. A., Corcelli, S. A., Skinner, J. L. & Tokmakoff, A. Collective Hydrogen Bond Reorganization in Water Studied with Temperature-Dependent Ultrafast Infrared Spectroscopy. *J. Phys. Chem. B* **115**, 5604-5616, doi:10.1021/jp111434u (2011).

8 Jungwirth, P. & Tobias, D. J. Surface effects on aqueous ionic solvation: A molecular dynamics simulation study of NaCl at the air/water interface from infinite dilution to saturation. *The Journal of Physical Chemistry B* **104**, 7702-7706 (2000).

9 Benjamin, I. Theoretical study of ion solvation at the water liquid-vapor interface. *J. Chem. Phys.* **95**, 3698-3709, doi:10.1063/1.460821 (1991).

10 Sitzmann, E. V. & Eisenthal, K. B. Picosecond dynamics of a chemical reaction at the air-water interface studied by surface second harmonic generation. *J. Phys. Chem.* **92**, 4579-4580, doi:10.1021/j100327a004 (1988).

11 McFearin, C. L. & Richmond, G. L. The Role of Interfacial Molecular Structure in the Adsorption of Ions at the Liquid-Liquid Interface. *J. Phys. Chem. C* **113**, 21162-21168, doi:10.1021/jp906616c (2009).

12 Garrett, B. C. Chemistry. Ions at the air/water interface. *Science* **303**, 1146-1147, doi:10.1126/science.1089801 (2004).

13 Culp, J. T., Park, J.-H., Stratakis, D., Meisel, M. W. & Talham, D. R. Supramolecular Assembly at Interfaces: Formation of an Extended Two-Dimensional Coordinate Covalent Square Grid Network at the Air−Water Interface. *Journal of the American Chemical Society* **124**, 10083-10090, doi:10.1021/ja026312e (2002).

14 Kuzmenko, I. *et al.* Design and Characterization of Crystalline Thin Film Architectures at the Air−Liquid Interface: Simplicity to Complexity. *Chemical Reviews* **101**, 1659-1696, doi:10.1021/cr990038y (2001).

15 Conway, B. E., Bockris, J. O. M. & Ammar, I. A. Dielectric constant of the solution in the diffuse and Helmholtz double layers at a charged interface in aqueous solution. *Trans. Faraday Soc.* **47**, 756-766, doi:10.1039/tf9514700756 (1951).

16 Chandra, A. Static dielectric constant of aqueous electrolyte solutions: Is there any dynamic contribution? *J. Chem. Phys.* **113**, 903-905, doi:10.1063/1.481870 (2000).

17 Palmer, L. S., Cunliffe, A. & Hough, J. M. Dielectric constant of water films. *Nature* **170**, 796, doi:10.1038/170796a0 (1952).

18 Medders, G. R. & Paesani, F. Dissecting the Molecular Structure of the Air/Water Interface from Quantum Simulations of the Sum-Frequency Generation Spectrum. *J. Am. Chem. Soc.* **138**, 3912-3919, doi:10.1021/jacs.6b00893 (2016).

19 Poli, E., Jong, K. H. & Hassanali, A. Charge transfer as a ubiquitous mechanism in determining the negative charge at hydrophobic interfaces. *Nat. Commun.* **11**, 901, doi:10.1038/s41467-020-14659-5 (2020).

20 Du, Q., Freysz, E. & Shen, Y. R. Surface vibrational spectroscopic studies of hydrogen bonding and hydrophobicity. *Science* **264**, 826-828, doi:10.1126/science.264.5160.826 (1994).

21 Kuo, I. F. W. & Mundy, C. J. An ab initio molecular dynamics study of the aqueous liquid-vapor interface. *Science* **303**, 658-660, doi:10.1126/science.1092787 (2004).

22 Stiopkin, I. V. *et al.* Hydrogen bonding at the water surface revealed by isotopic dilution spectroscopy. *Nature* **474**, 192-195, doi:10.1038/nature10173 (2011).

23 Reddy, S. K. *et al.* Bulk Contributions Modulate the Sum-Frequency Generation Spectra of Water on Model Sea-Spray Aerosols. *Chem* **4**, 1629-1644, doi:10.1016/j.chempr.2018.04.007 (2018).

24 Pezzotti, S., Galimberti, D. R., Shen, Y. R. & Gaigeot, M.-P. Structural definition of the BIL and DL: A new universal methodology to rationalize non-linear χ (2)(ω) SFG signals at charged interfaces, including χ (3)(ω) contributions. *Physical Chemistry Chemical Physics* **20**, 5190-5199 (2018).

25 Fan, Y., Chen, X., Yang, L., Cremer, P. S. & Gao, Y. Q. On the Structure of Water at the Aqueous/Air Interface. *The Journal of Physical Chemistry B* **113**, 11672-11679, doi:10.1021/jp900117t (2009).

26 Kühne, T. D., Pascal, T. A., Kaxiras, E. & Jung, Y. New Insights into the Structure of the Vapor/Water Interface from Large-Scale First-Principles Simulations. *The Journal of Physical Chemistry Letters* **2**, 105-113, doi:10.1021/jz101391r (2011).

27 Dang, L. X. & Chang, T.-M. Molecular dynamics study of water clusters, liquid, and liquid-vapor interface of water with many-body potentials. *J. Chem. Phys.* **106**, 8149-8159, doi:10.1063/1.473820 (1997).

28 Chacon, E., Tarazona, P. & Alejandre, J. The intrinsic structure of the water surface. *J. Chem. Phys.* **125**, 014709/014701-014709/014710, doi:10.1063/1.2209681 (2006).

29 Dang, L. X. & Chang, T.-M. Many-body interactions in liquid methanol and its liquid/vapor interface: A molecular dynamics study. *The Journal of chemical physics* **119**, 9851-9857 (2003).

30 Schmid, G. M., Hurd, R. M. & Snavely, E. S., Jr. Effects of electrostatic fields on the surface tension of salt solutions. *J. Electrochem. Soc.* **109**, 852-858, doi:10.1149/1.2425568 (1962).

31 Hayes, C. F. Water-air interface in the presence of an applied electric field. *J. Phys. Chem.* **79**, 1689-1693, doi:10.1021/j100583a016 (1975).

32 Pethica, B. A. Electric Field Effects on Air/Solution Interfaces. *Langmuir* **14**, 3115-3117, doi:10.1021/LA971142I (1998).

33 Jiang, Q., Chiew, Y. C. & Valentini, J. E. Electric field effects on the surface tension of air/solution interfaces. *Colloids Surf., A* **83**, 161-166, doi:10.1016/0927-7757(94)80099-5 (1994).

34 Hurd, R. M., Schmid, G. M. & Snavely, E. S., Jr. Electrostatic fields, their effect on the surface tension of aqueous salt solutions. *Science* **135**, 791-792, doi:10.1126/science.135.3506.791 (1962).

35 Laanait, N. *et al.* Tuning ion correlations at an electrified soft interface. *Proc. Natl. Acad. Sci. U. S. A.* **109**, 20326-20331, S20326/20321-S20326/20326, doi:10.1073/pnas.1214204109 (2012).

36 Wang, H., Borguet, E. & Eisenthal, K. B. Polarity of Liquid Interfaces by Second Harmonic Generation Spectroscopy. *J. Phys. Chem. A* **101**, 713-718, doi:10.1021/JP962074W (1997).

37 Shen, Y. R. *The Principles of Nonlinear Optics* (Wiley, New York, 1984)

38 Corn, R. M. & Higgins, D. A. Optical second harmonic generation as a probe of surface chemistry. *Chem. Rev.* **94**, 107-125, doi:10.1021/cr00025a004 (1994).

39 Zhao, X., Ong, S. & Eisenthal, K. B. Polarization of water molecules at a charged interface. Second harmonic studies of charged monolayers at the air/water interface. *Chem. Phys. Lett.* **202**, 513-520, doi:10.1016/0009-2614(93)90041-X (1993).

40 Gouy. Constitution of the Electric Charge at the Surface of an Electrolyte. *J. physique, [4]* **9**, 457-467 (1910).

41 Chapman, D. L. A contribution to the theory of electrocapillarity. *Philosophical Magazine* **25**, 475-481 (1913).

42 Shin, S. & Willard, A. P. Three-Body Hydrogen Bond Defects Contribute Significantly to the Dielectric Properties of the Liquid Water-Vapor Interface. *J Phys Chem Lett* **9**, 1649-1654 (2018).

43 Shin, S. & Willard, A. P. Water's Interfacial Hydrogen Bonding Structure Reveals the

Effective Strength of Surface-Water Interactions. *J Phys Chem B* **122**, 6781-6789 (2018).
44 Nihonyanagi, S. *et al*. Unified Molecular View of the Air/Water Interface Based on Experimental and Theoretical χ(2) Spectra of an Isotopically Diluted Water Surface. *J. Am. Chem. Soc.* **133**, 16875-16880, doi:10.1021/ja2053754 (2011).
45 Nihonyanagi, S., Mondal, J. A., Yamaguchi, S. & Tahara, T. Structure and dynamics of interfacial water studied by heterodyne-detected vibrational sum-frequency generation. *Annu. Rev. Phys. Chem.* **64**, 579-603, doi:10.1146/annurev-physchem-040412-110138 (2013).
46 Shen, Y. R. Phase-sensitive sum-frequency spectroscopy. *Annu. Rev. Phys. Chem.* **64**, 129-150, doi:10.1146/annurev-physchem-040412-110110 (2013).
47 Ishiyama, T., Imamura, T. & Morita, A. Theoretical Studies of Structures and Vibrational Sum Frequency Generation Spectra at Aqueous Interfaces. *Chem. Rev. (Washington, DC, U. S.)* **114**, 8447-8470, doi:10.1021/cr4004133 (2014).
48 Ishiyama, T. & Morita, A. Vibrational Spectroscopic Response of Intermolecular Orientational Correlation at the Water Surface. *J. Phys. Chem. C* **113**, 16299-16302, doi:10.1021/jp9060957 (2009).
49 Ishiyama, T. & Morita, A. Analysis of anisotropic local field in sum frequency generation spectroscopy with the charge response kernel water model. *J. Chem. Phys.* **131**, 244714/244711-244714/244717, doi:10.1063/1.3279126 (2009).
50 Pieniazek, P. A., Tainter, C. J. & Skinner, J. L. Surface of liquid water. Three-body interactions and vibrational sum-frequency spectroscopy. *J. Am. Chem. Soc.* **133**, 10360-10363, doi:10.1021/ja2026695 (2011).

Methods:

1.1 Materials and Sample Preparation

Milli-Q (>18.0 MΩ) ultra-pure water was used as a neat water source without the addition of any other chemicals. The purity of the neat water was confirmed by measuring the surface tension of water. Our measurements of (72.15±0.08) mN/m at (23.1±0.5)°C are in agreement with previous literature[51,52]. The pH was monitored; before the experiment, between 5-15 minutes after obtaining water from our Milli-Q system, the pH was measured to be 6.29 ± 0.05 at (23.1 ± 0.5)°C (**Table S1**). The pH of water then dropped to (5.80 ± 0.08) after 5 to 6 hours of atmospheric exposure due to CO_2 absorption as is expected. Second harmonic measurement began 30 mins after obtaining the water samples from the Milli-Q system. Voltage experiments were completed over an ~5.5 to 6.5 hour time period. The observed decrease of pH with time was shown to be undetectable by second harmonic measurement; reversing the order and randomization of experiments verified this conclusion among other controls.

1.2 Second Harmonic Generation and Applied Voltage Instrumentation

1.2.1 Instrumentation. A custom-built Second Harmonic Generation (SHG) system with a reference channel was utilized for these experiments (**Fig. S1**). The SHG system consists of a Ti:sapphire oscillator (Tsunami, Spectra-Physics) with a wavelength centered at 805 nm, a half width half maximum of 10 nm, a sub 50 fs pulse width, and a repetition rate of 82 MHz. The average output power from the Tsunami is around 860 mW. The oscillator is pumped by a continuous wave (CW) solid state diode laser (Millennia Vs, Spectra-Physics) with a pump power of 5 W. The output laser beam is separated by a ratio of 90/10 by a beam splitter, where 90% of the laser power is introduced to the sample channel and the other 10% of the beam is used in the reference channel (BBO nonlinear optical crystal).The sample channel consists of four dielectric mirrors (BB1-E03, Thorlabs), one Glan-laser polarizer (10GL08AR.16, Newport), one half-wave plate (10RP52-2B, Newport), one plano-convex lens with a focal length of 75 mm (LA1608-B, Thorlabs) and one 690 nm long-pass filter (690LP RapidEdge, Omega Optical). The laser pulses reflect off of the liquid surface with an angle of 67.2° with respect to the surface normal.

The purpose of using the polarizer, half-wave plate, and long-pass filter is to purify the input and detected polarizations, and when used after the sample reflection, these optics remove unwanted second harmonic light produced by optical components. The average power before exciting the sample was 550 mW. The interfacial second harmonic signal has a wavelength of 403 nm, which is generated by the aqueous sample. The fundamental beam from the reference channel is attenuated by three neutral density filters, where the frequency of the fundamental beam is doubled by a BBO crystal, and the rest of the fundamental light is blocked by a 700 nm short-pass filter (Thor Labs, FES 700). The transmitted 403 nm beam from the reference channel combines with the signal beam path by a silica plate slightly angled for optimization. Next, the sample and reference channel beams are focused by a 50 mm focusing lens (LA1131-B, Thorlabs) into the detector with slit open (2500 μm) to avoid clipping of the SHG signal.

The detection system is comprised of a Czerny-Turner type monochromator (Shamrock SR303i, Andor Tech.) and an EMCCD (Newton DU970N-BV EMCCD, Andor Tech.). The monochromator grating is 68x68 μm with a groove density of 300 lines/mm. The CCD consists of 1600x200 pixel array (Blazed at 500 nm), with 16x16 μm pixel size. Electron multiplying was set to 200 times to enhance the signal count and the thermal electric cooling was set at -60 °C to reduce thermal noise. Normalization of the second harmonic signal was done as a ratio of the reflected signal from the sample of interest to that of the neat water surface at zero applied potential (0 V) noting that the neat water signal to itself is then defined as an intensity of unity.

The high voltage set up is comprised of two electrodes: the DC-powered steel electrode (25x20 x0.40 mm^3), located in the air-phase, and the grounded parallel platinum counter electrode

(25x22x0.10 mm^3, Fisher Scientific) in the condensed-phase. The applied external potential range was negative (-) 5 to positive (+) 5 kV, where the applied electric field was normal to the water-air interface. The distance between the air-phase electrode and the water surface was maintained at 5 mm, whereas the condensed-phase electrode was maintained at 5 mm below the water surface for fixed airgap experiments. The effect of the external potential on the water-air interface was also studied by changing the airgap between the water surface and the air-electrode from 5 mm to 27 mm with a constant external potential of 3 kV.

1.2.2 Second Harmonic Intensity and Nonlinear Susceptibility. The second harmonic intensity of the water-air interface was collected using the custom built second harmonic instrument described above using pp polarization. We collected both the sample and reference channel intensities. The reflected second harmonic signal intensity, $I(2\omega)$, on the neat water surface can be written in terms of the incoming laser intensity, $I(\omega)$, as follows:[53-55]

$$I(2\omega) = \frac{32\pi^3\omega^2 \sec^2\beta}{c_0^3 n_1(\omega) n_1(\omega) n_1(2\omega)} \left|\chi_{eff}^{(2)}\right|^2 I^2(\omega) \quad (1)$$

Where, c_0, $n_i(\omega_i)$ and β denote the speed of light in vacuum, refractive index of the medium, and incident angle of the incoming laser normal to the water surface, respectively. Here, $\chi_{eff}^{(2)}$ indicates the effective second-order susceptibility of the water surface which provides information about the alignment of surface and subsurface water molecules in the z-direction. Overall, the second harmonic signal provides information about the dipole moment of interfacial asymmetric molecules.

The dependence of second harmonic signal intensity on surface potential and surface charges are well established and is attributed to the bulk $\chi^{(3)}$ effect.[56-61] This third-order contribution was first reported at the silica/water interface using the second harmonic spectroscopy by Eisenthal *et al.*[56] We note that the $\chi^{(3)}$ is likely contributing to SHG signal and due to the applied electric field.

1.2.3 Replicate Second Harmonic Measurements: Applying Varying Potentials at a Fixed Airgap. The second harmonic intensities of neat water with or without external potentials were normalized with respect to neat water intensity at zero external potential. **Fig. S2** shows the normalized second harmonic intensities of the water surface with the applied external potentials ranging from negative (-) 5 kV to positive (+) 5 kV. A minimum of six replicate measurements were performed for each data point presented. Altogether, we performed six separate sets of experiment to justify the robustness of the measurement. The average of the normalized second harmonic intensities of experiments 1, 2, 3, 4, 5 and 6 are presented with one standard deviation.

2.1 Control Experiments

2.1.1 Applying a Fixed Potentials with Varying Airgap: Second Harmonic Response. The variation of the water surface second harmonic intensity was investigated under a fixed external potential with varying airgaps ranging from 0.5 to 2.7 cm. The airgap was defined as the distance between the water surface and the air-electrode. We observe a monotonic decrease in experimental signal intensity with increasing separation distance between the air electrode and the water interface, presumably due to the associated decrease in electric fields. **Fig. S3** shows the normalized second harmonic intensity of water at +3 and -3 kV external electric potential with the different airgaps.

2.1.2 Sum Frequency Generation spectra of hydrogen bonded OH and free OH stretch regions under applied potential. Sum frequency measurements were done in the hydrogen bonded OH and free OH stretch regions to understand the impact of applied potential on water orientation through the sum frequency transition moment of water molecules at water-air interface. **Figs. S4 and S5** shows the sum frequency spectra of hydrogen bonded OH (ssp polarization) and free OH stretch regions (ssp and ppp polarization). The spectra under applied external potentials show no discernable difference with respect to the zero biased spectrum (zero applied external potential) in all cases.

At the water-air interface, free hydroxyl moiety contributes 25% to the total surface water molecules. Thus, it was important to probe the free

OH stretch region along with the broad band hydrogen bonded stretch region (3200 cm^{-1}-to-3600 cm^{-1}). The free OH stretching mode can be studied experimentally by a sharp peak at ~3700 cm^{-1} using the vibrational sum frequency spectroscopy [62,63]. The high voltage experimental setup used in these experiments is similar to that of the second harmonic measurements. The distance between the air-phase electrode and the water surface was maintained at 1 cm, whereas the condensed-phase electrode was maintained at 0.4 cm below the water surface (**Fig. S6**). The experiments for the hydrogen-bonded OH region were done in ssp polarization and that for the free OH region were completed in two different polarization combinations of ssp and ppp. The polarization combinations are listed in the order of decreasing frequency (SF, Vis, IR). Light polarized perpendicular to the incident plane is referred to as s polarized, whereas light polarized parallel to the incident plane is p polarized. The vibrational modes that contribute to a particular polarization combination depend on the polarization of the infrared field and the direction of the infrared and Raman transition moments. The ssp polarization combination accesses vibrational modes primarily with dipole transition moments that have components perpendicular to the surface plane. Whereas, vibrational modes with components that are both perpendicular and parallel to the surface plane will be present in ppp polarization [64]. Thus, the free OH sum frequency responses measured with ssp and ppp polarization combinations provide information about orientation [65,66]. **Figs. S4** and **S5** compare the sum frequency signal for hydrogen bonded OH (ssp) and of free OH stretch region (ssp and ppp), respectively. The measured sum frequency spectra for both spectral regions show no appreciable change under applied external potential in the range of negative (-) 5 kV to positive (+) 5 kV. Within the signal to noise of our sum frequency instrument, this implies negligible change of the hydrogen bond network and overall orientation of water molecules under current experimental conditions.

The details of the broadband sum frequency generation spectrometer set up used for this study were previously reported [67-69]. In brief, a regenerative Ti:sapphire amplifier (Spitfire Ace, Spectra-Physics) seeded with a sub-50 fs 800 nm pulse from a Ti:sapphire oscillator provides an ~3.5 W beam of 75 fs pulses and 1 kHz repetition rate. The amplified beam is then directed through a 50:50 beam splitter. One half of the beam is used to pump an optical parametric amplification system (TOPAS-C, Light Conversion), that is coupled to a non-collinear difference frequency generator (NDFG, Light Conversion) to generate the broadband infrared beam. The other half of the beam is spectrally narrowed to a FWHM of 12 cm^{-1} by an etalon (SLS Optics, United Kingdom) and is used as the visible 797 nm beam. The infrared and the visible beams are co-propagating and fall on the sample surface at angle from the surface normal of 60 and 50 degrees, respectively. The visible beam is focused approximately 1 cm after the surface with a BK7 lens (25 cm FL) and the infrared beam is focused on the sample surface with a CaF_2 lens (15 cm FL). The sum frequency signal is collected in the reflected direction by a spectrometer (IsoPlane SCT 320, Princeton Instruments) and a liquid nitrogen cooled CCD (PyLoN, 1340 × 400 pixels, Princeton Instruments). The data for H-bonded OH region were obtained with 60 seconds integration time with 5 averages, and plotted after background subtraction and normalization with respect to non-resonant signal from a gold mirror. The sum frequency spectra for the free OH spectral region were obtained with 20 sec integration time and 3 averages and plotted after background subtraction. The IR laser profile and energies of visible and IR beam were periodically measured and was stable throughout the measurement.

2.2 Theoretical calculations

2.2.1 Gaussian Field Model. The characteristic feature of the experimental results in this system is a minimum in the spectroscopic response of the air-water interface at a non-zero applied field. Here, we sketch a simple Gaussian model for the interfacial polarization field that provides a compelling microscopic interpretation of the experimental result. It is known and well accepted that even under zero applied potential, water molecules at the air-water interface carry an intrinsic polarization due to broken longitudinal symmetry at the interface. To low order, we expect fluctuations around the preferred polarization at any field to carry Gaussian statistics.

Equipped with these physical considerations, we postulate the following Hamiltonian for the z-component of the polarization variable $\pi_z$at the interface,

$$H[\pi_z] = \frac{k}{2}[\pi_z - \pi_z^*]^2 - \lambda \cdot \pi_z E_z$$

where π_z is the z-component (taken as normal to the interface by convention) of the plane-averaged dielectric polarization at the interface, π_z^* is the preferred value of the polarization at zero applied field, k is the energy scale associated with interfacial polarization fluctuations, E_z is the z -component of the applied interfacial electric field, and λ is a coupling constant quantifying the tendency of the applied electric field to align water dipoles at the interface. Mathematically, adding a linear coupling to a parabolic Hamiltonian simply translates the parabola to a new preferred polarization value. Completing the square results in an equivalent expression for the Hamiltonian that makes this field-dependent shift in the preferred polarization obvious,

$$H[\pi_z] = \frac{k}{2}\left[\pi_z - \left(\pi_z^* - \frac{\lambda E_z}{k}\right)\right]^2 - \lambda E_z\left(1 + \frac{\lambda E_z}{2k}\right)$$

At this point, we address units. For the sake of easily estimating parameters from molecular simulation, we track the polarization field π_z in fictive $\cos\theta$ units. One can glean the quantity in these units by normalizing the interfacial polarization vector by an arbitrary polarization scale, and then dotting the normalized vector into the interface normal. The Hamiltonian above is Gaussian, and so we can simply read off the mean from the offset in the quadratic term. Specifically, the mean polarization goes as,

$$\langle \pi_z \rangle = \pi_z^* - \frac{\lambda E_z}{k}$$

The spectroscopic response of the interface is proportional to the square of the mean interfacial polarization, plus any background signal,

$$\text{Response}[E_z] = B + A \cdot \langle \pi_z \rangle^2$$

where B is the magnitude of background signal, and A is a proportionality constant relating the interfacial polarization to the spectroscopic response, both of which are assumed to be constant at all values of the applied interfacial field. Since the experimental data is normalized to the zero-field value, we can factor out the background response and eliminate it as an overall constant, leaving us with,

$$\text{NormResponse}[E_z] = 1 + \left(\frac{A}{B}\right) \cdot \left[\pi_z^* - \left(\frac{\lambda}{k}\right) E_z\right]^2$$

where the response carries a parametric dependence on the quantities π_z^*, λ/k , and A/B, which need to be estimated from simulation data.

First, the quantity $\langle \pi_z \rangle$ simply serves to scale the interfacial polarization into spectroscopic signal, and is assumed to be independent of the applied field. Since we can only access the value of $\langle \pi_z \rangle$ directly from simulation data, without loss of generality, we set $A/B = 1$. We choose to estimate the remaining model parameters, π_z^*, and λ/k using insight provided by simulations of an interface between water and a perfectly volume-excluding wall that can carry a surface charge. The surface charge density at the wall, σ_q, can be mapped to an effective interfacial electric field in the simulation data. **Fig. S7** shows a relationship between the surface charge density at the wall (measured in arbitrary units) vs. the computed interfacial electric field (in units of V/Å). The slope gleaned from this linear relationship is 0.65 V/Å, implying that the interfacial electric field increases by 0.65 V/Å for each σ_q unit.

As worked out in the section above on field magnitudes, the maximal applied experimental field is roughly 0.44 V/Å. Hence, simulations conducted with wall charge densities up to $\sigma_q \approx 0.68$ are in correspondence with the experimental field magnitudes. Trajectory analysis on the molecular dynamics simulation data allows for quantification of the orientational distributions of water molecules, resolved as a function of distance from the interface. **Fig. S8A** shows distributions of the interfacial polarization as a function of the wall charge density σ_q. **Fig. S8B** shows the modal value of the interfacial polarization as a function of σ_q. We choose to use the mode as a summary statistic for the distribution because it is more robust to the large tails of the distributions easily identifiable in **Fig. S8A**.

With the data in these two plots in hand, we estimate the values of the model parameters. The

parameter λ/k describes how much the preferred polarization value moves with the applied interfacial field. If we employ the modal value of the $\cos\theta$ distribution as a proxy for the preferred polarization value and estimate the interfacial electric field in units of σ_q, then we can estimate λ/k from the data available in **Fig. S8B**. Specifically, λ/k is the slope of the response curve; we have a decision to make as to the range of σ_q values over which we fit this response slope. If we choose the dynamic range of $\sigma_q \in [-0.1, 0.1]$for slope estimation from **Fig. S8B**, then we have $\lambda/k \approx 0.75$ in the aforementioned units. We can estimate the value of π_z^*, by examining the modal value of the interfacial polarization at zero externally applied field. Reading off the value at $\sigma_q = 0$ in **Fig. S8B** yields the estimate $\pi_z^* \approx 0.18$.

2.2.2 Models for Experimental Field Magnitudes. In the experimental apparatus, the applied voltage between two parallel plates can reach as high as 5 kV. Naively, if we were to drop this entire voltage over the 5 mm water layer as if in a parallel-plate capacitor, we would obtain a paltry (on a molecular scale) field of $E \approx 1 \times 10^{-4}$ V/Å. Insights from simulation data, and simple thermodynamic arguments (the field is far lower than the thermal field $E_{\text{thermal}} = k_B T/[e \times 1\,\text{Å}]$) suggest that the field experienced at the interface is orders of magnitude greater than this simple parallel-plate capacitor argument may suggest.

We advance the hypothesis that elevated interfacial fields are present in the experiment due to formation of an electrochemical double-layer near the air-water interface by the hydronium and hydroxide ions present in water at the experimental pH. The experiment is conducted at pH = 6.25, implying a hydronium concentration $c_{\text{Hydronium}} = 5.6 \times 10^{-7}\text{mol/L}$ and a hydroxide concentration $c_{\text{Hydroxide}} = 5.6 \times 10^{-7}\text{mol/L}$. The relevant length scale for formation of an electrochemical double layer is the Debye length,

$$\ell_{\text{Debye}} = \left[\frac{\epsilon k_B T}{\sum_j c_j q_j^2}\right]^{1/2}$$

where ϵ is the dielectric constant of neat water, k_B is the Boltzmann constant, T is the temperature, the sum runs over all ionic species j, and c_j and q_j denote the concentration and charge carried by the ionic species, respectively. At the experimental conditions, the Debye length is $\ell_{\text{Debye}} = 565$ nm. If we assume that half the potential drop is dropped over the air-water double-layer (the other half is dropped over the grounded electrode-water double layer), then the maximal accessible interfacial field in experiment is roughly 0.44 V/Å.

2.2.3 Molecular Dynamics Simulation Methods. The molecular dynamics simulations employed in this work model water molecules using an atomistic molecular mechanics force field. The water molecules are in contact with an idealized wall of volume-excluding spheres carrying a constant surface charge, which is variable across different simulations. Orientational statistics of water molecules are computed relative to the local instantaneous interface, a construct developed by Willard and Chandler which factors out long-wavelength capillary wave-like fluctuations from the interface.[70] The distributions and values of order parameters from simulations presented in Figs. S7A and S7B are time averages taken over an entire trajectory of simulation.

References

51 Vargaftik, N. B., Volkov, B. N. & Voljak, L. D. International tables of the surface tension of water. *Journal of Physical and Chemical Reference Data* **12**, 817-820 (1983).

52 Berry, J. D., Neeson, M. J., Dagastine, R. R., Chan, D. Y. C. & Tabor, R. F. Measurement of surface and interfacial tension using pendant drop tensiometry. *Journal of colloid and interface science* **454**, 226-237 (2015).

53 Rao, Y., Tao, Y.-s. & Wang, H.-f. Quantitative analysis of orientational order in the molecular monolayer by surface second harmonic generation. *The Journal of chemical physics* **119**, 5226-5236 (2003).

54 Zhuang, X., Miranda, P. B., Kim, D. & Shen, Y. R. Mapping molecular orientation and

conformation at interfaces by surface nonlinear optics. *Physical Review B* **59**, 12632 (1999).
55 Bian, H.-t., Feng, R.-r., Xu, Y.-y., Guo, Y. & Wang, H.-f. Increased interfacial thickness of the NaF, NaCl and NaBr salt aqueous solutions probed with non-resonant surface second harmonic generation (SHG). *Phys. Chem. Chem. Phys.* **10**, 4920-4931, doi:10.1039/b806362a (2008).
56 Ong, S., Zhao, X. & Eisenthal, K. B. Polarization of water molecules at a charged interface: second harmonic studies of the silica/water interface. *Chemical Physics Letters* **191**, 327-335 (1992).
57 Yan, E. C. Y., Liu, Y. & Eisenthal, K. B. New method for determination of surface potential of microscopic particles by second harmonic generation. *The Journal of Physical Chemistry B* **102**, 6331-6336 (1998).
58 Geiger, F. M. Second harmonic generation, sum frequency generation, and $\chi(3)$: dissecting environmental interfaces with a nonlinear optical Swiss Army knife. *Annual review of physical chemistry* **60**, 61-83 (2009).
59 Salafsky, J. S. & Eisenthal, K. B. Protein adsorption at interfaces detected by second harmonic generation. *The Journal of Physical Chemistry B* **104**, 7752-7755 (2000).
60 Joutsuka, T., Hirano, T., Sprik, M. & Morita, A. Effects of third-order susceptibility in sum frequency generation spectra: a molecular dynamics study in liquid water. *Physical Chemistry Chemical Physics* **20**, 3040-3053 (2018).
61 Ishiyama, T., Shirai, S., Okumura, T. & Morita, A. Molecular dynamics study of structure and vibrational spectra at zwitterionoic lipid/aqueous KCl, NaCl, and CaCl2 solution interfaces. *The Journal of chemical physics* **148**, 222801 (2018).
62 Jubb, A. M., Hua, W. & Allen, H. C. Environmental chemistry at vapor/water interfaces: insights from vibrational sum frequency generation spectroscopy. *Annu. Rev. Phys. Chem.* **63**, 107-130, doi:10.1146/annurev-physchem-032511-143811 (2012).
63 Thiel, S., Hammerl, G., Schmehl, A., Schneider, C. W. & Mannhart, J. Tunable Quasi-Two-Dimensional Electron Gases in Oxide Heterostructures. *Science* **313**, 1942-1945, doi:10.1126/science.1131091 (2006).
64 Conboy, J. C., Messmer, M. C. & Richmond, G. L. Investigation of Surfactant Conformation and Order at the Liquid-Liquid Interface by Total Internal Reflection Sum-Frequency Vibrational Spectroscopy. *J. Phys. Chem.* **100**, 7617-7622, doi:10.1021/JP953616X (1996).
65 Feng, R.-R., Guo, Y. & Wang, H.-F. Reorientation of the "free OH" group in the top-most layer of air/water interface of sodium fluoride aqueous solution probed with sum-frequency generation vibrational spectroscopy. *J. Chem. Phys.* **141**, 18C507/501-518C507/510, doi:10.1063/1.4895561 (2014).
66 Gan, W., Wu, D., Zhang, Z., Feng, R.-r. & Wang, H.-f. Polarization and experimental configuration analyses of sum frequency generation vibrational spectra, structure, and orientational motion of the air/water interface. *J. Chem. Phys.* **124**, 114705/114701-114705/114715, doi:10.1063/1.2179794 (2006).
67 Adams, E. M. *et al.* Surface organization of a DPPC monolayer on concentrated SrCl2 and ZnCl2 solutions. *Phys. Chem. Chem. Phys.* **18**, 32345-32357, doi:10.1039/C6CP06887A (2016).
68 Adams, E. M. *et al.* Sodium-carboxylate contact ion pair formation induces stabilization of palmitic acid monolayers at high pH. *Phys Chem Chem Phys* **19**, 10481-10490 (2017).
69 Lin, L. *et al.* Iron(III) Speciation Observed at Aqueous and Glycerol Surfaces: Vibrational Sum Frequency and X-ray. *J. Am. Chem. Soc.* **141**, 13525-13535, doi:10.1021/jacs.9b05231 (2019).
70 Willard, A. P. & Chandler, D. Instantaneous Liquid Interfaces. *The Journal of Physical Chemistry B* **114**, 1954-1958, doi:10.1021/jp909219k (2010).

Acknowledgments: "This work was supported by the U.S. Department of Energy, Office of Science, Basic Energy Sciences, under Awards # DE-SC0016381 and # DE-SC0018094, Allen and

Willard Labs, respectively. HCA and KKR acknowledge Prof. A. Co for helpful discussions.

Author contributions:
H.C.A, A.P.W. and K.K.R. conceived the study and designed the experiments. K.K.R. and K.C.N. performed SHG setup. K.K.R. carried out SHG experiment, SHG characterization and high voltage set up. A.L. performed MD simulations. A.S. and K.K.R. performed SFG characterization. H.C.A, A.P.W., A.L. and K.K.R. wrote the paper with help from all the authors.

Competing Interests
The authors declare no competing interests.

Additional information

Extended data is available for this paper at _____

Supplementary information is available for this paper at _...

Correspondence and requests for materials should be addressed to H.C.A and A.P.W. for experimental and theory detail, respectively.

Peer review information *Nature Chemistry* thanks the anonymous reviewers for their contribution to the peer review of this work.

Reprints and permissions information is available at …